Title

Mechanisms for hydroxyl radical production and arsenic removal in sulfur-vacancy greigite (Fe3S4)

Journal

Journal of Colloid and Interface Science, 606(Pt 1)

ISSN

0021-9797

Authors

Liu, Wei
Liu, Jia
Zhou, Peipei
et al.

Publication Date

2022

DOI

10.1016/j.jcis.2021.08.072

Peer reviewed

Journal of Colloid and Interface Science 606 (2022) 688–695

Contents lists available at ScienceDirect

Journal of Colloid and Interface Science

journal homepage: www.elsevier.com/locate/jcis

Mechanisms for hydroxyl radical production and arsenic removal in sulfur-vacancy greigite (Fe_3S_4)

Wei Liu [a,c], Jia Liu [a], Peipei Zhou [a], Randy A. Dahlgren [d], Xuedong Wang [a,b,*]

[a] Zhejiang Provincial Key Laboratory of Watershed Science and Health, College of Public Health and Management, Wenzhou Medical University, Wenzhou 325035, China
[b] National and Local Joint Engineering Laboratory of Municipal Sewage Resource Utilization Technology, School of Environmental Science and Engineering, Suzhou University of Science and Technology, Suzhou 215009, China
[c] Key Laboratory for Green Chemical Process of Ministry of Education, School of Chemical Engineering and Pharmacy, Wuhan Institute of Technology, Wuhan 430205, China
[d] Department of Land, Air and Water Resources, University of California, Davis, CA 95616, United States

GRAPHICAL ABSTRACT

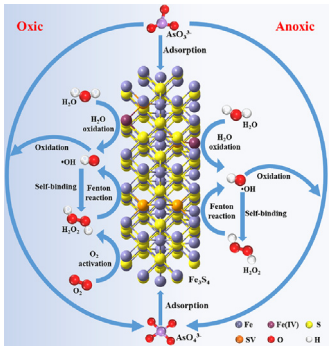

ARTICLE INFO

Article history:
Received 17 May 2021
Revised 8 August 2021
Accepted 9 August 2021
Available online 14 August 2021

Keywords:
Greigite (Fe_3S_4)
Sulfur-vacancy
Oxic/anoxic
Reactive oxygen species (ROS)
Arsenic (As(III))

ABSTRACT

Herein, we systematically investigated the mechanisms of ·OH production and arsenic (As(III)) oxidation induced by sulfur vacancy greigite (Fe_3S_4) under anoxic and oxic conditions. Reactive oxygen species analyses revealed that sulfur vacancy-rich Fe_3S_4 (SV-rich Fe_3S_4) activated molecular oxygen to produce hydrogen peroxide (H_2O_2) via a two-electron reduction pathway under oxic conditions. Subsequently, H_2O_2 was decomposed to ·OH via the Fenton reaction. Additionally, H_2O was directly oxidized to ·OH by surface high-valent iron (Fe(IV)) resulting from the abundance of sulfur vacancies in Fe_3S_4 under anoxic/oxic conditions. These differential ·OH-generating mechanisms of Fe_3S_4 resulted in higher ·OH production of SV-rich Fe_3S_4 compared to sulfur vacancy-poor Fe_3S_4 (SV-poor Fe_3S_4). Moreover, the ·OH production rate of SV-rich Fe_3S_4 under oxic conditions (19.3 ± 1.0 $\mu M \bullet h^{-1}$) was 1.6 times greater than under anoxic conditions (11.8 ± 0.4 $\mu M \bullet h^{-1}$). As(III) removal experiments and X-ray photoelectron spectra (XPS) showed that both ·OH production pathways were favorable for As(III) oxidation, and a higher concentration of As(V) was immobilized on the surface of SV-rich Fe_3S_4 under oxic conditions. This study provides new insights concerning ·OH production and environmental pollutants removal mechanisms on surface defects of Fe_3S_4 under anoxic and oxic conditions.

* Corresponding author at: Zhejiang Provincial Key Laboratory of Watershed Science and Health, College of Public Health and Management, Wenzhou Medical University, Wenzhou 325035, China.
E-mail address: zjuwxd@163.com (X. Wang).

https://doi.org/10.1016/j.jcis.2021.08.072
0021-9797/

1. Introduction

Hydroxyl radical (·OH) is a strong oxidant owing to its high standard reduction potential (2.8 eV), and plays a pivotal role in environmental chemistry, geochemistry, and life sciences [1]. For example, ·OH can directly mineralize organic pollutants and natural organic matter (NOM) to CO_2 [2], and alter microbial structure and metabolic processes [3]. Hydroxyl radicals also impact human health, such as ·OH formation as a byproduct of mineral oxidation that contributes to pneumoconiosis in coal miners [4]. Hydroxyl radicals are not only produced via photolysis of NOM in the atmosphere, surface waters and oceans, but also by redox reactions between naturally-occurring minerals and oxygen or water [5–8]. Thus, it is important to elucidate ·OH production mechanisms in natural environments.

Iron-based materials, including zero-valent iron (ZVI) and iron sulfides, are widely used as efficient activators for ·OH production ascribing to their redox reactivity [9–12]. Mechanisms for ·OH generation are a function of mineral structure and ambient environmental conditions. For instance, ZVI serves as an electron donor for molecular oxygen (O_2) activation via a two-electron transfer pathway to generate hydrogen peroxide (H_2O_2). Furthermore, structural ferrous ions (≡Fe(II)) in iron-based materials may first reduce O_2 to superoxide anions ($\cdot O_2^-$) via a single-electron transfer pathway, with the $\cdot O_2^-$ subsequently reduced to H_2O_2 via a single-electron transfer route [13–15]. The generated H_2O_2 then decomposes to ·OH by reaction with Fe(II) via the Fenton reaction. Moreover, contributions of these two O_2 activation pathways are mediated by competing ligands [12,16].

Recent studies verified the role of surface defects in iron minerals as efficient activation sites for ·OH production. For example, nonstoichiometric Fe(III) sites resulting from sulfur-deficient defects in pyrite directly oxidized H_2O to ·OH under anoxic conditions [17]. He et al. demonstrated that ·OH produced via reaction of Fe(III) and H_2O on pyrite under visible light irradiance and anoxic conditions resulted in antimony (Sb(III)) oxidation [18]. However, most natural minerals ordinarily experience alternating oxic and anoxic conditions, ascribing to the strong O_2 perturbations in subsurface environments [19]. Thus, past studies provide evidence for ·OH production by both O_2 activation and H_2O oxidation pathways in natural environments under oxic and anoxic conditions. For instance, Yuan et al.[20] systematically evaluated the mechanism of ·OH production from pyrite oxidation under oxic and anoxic conditions, and documented that more ·OH was generated from H_2O oxidation on sulfur-deficient sites of pyrite surfaces under anoxic conditions. The authors demonstrated that the predominant ·OH generation pathway was identified as the two-electron transfer route under oxic conditions [20].

Greigite (Fe_3S_4), as an intermediate phase on the transformation pathway of FeS to pyrite, forms during early diagenetic stages involving sedimentary sulfate reduction [21–23]. Given the important role of Fe_3S_4 in environmental chemistry and geochemistry, many studies explored the effects of Fe_3S_4 on the fate and transport of environmental compounds. For example, heavy metals such as antimony (Sb(III)/Sb(V)) and lead (Pb(II)) could be efficient adsorbed on Fe_3S_4 surface, which significantly decreased their mobility and toxicity [24,25]. Moreover, hydrogen peroxide (H_2O_2) and peroxydisulfate ($S_2O_8^{2-}$) were adsorbed on the surface of Fe_3S_4 where they were sequentially activated to ·OH and $\cdot SO_4^{2-}$ for bisphenol and atrazine degradation [26,27]. Thus, naturally-occurring Fe_3S_4 may impact several related remediation processes of environmental pollutants.

Our previous studies demonstrated that Fe_3S_4 efficiently reduced Cr(VI) and roxarsone, owing to the coupled reductive abilities of structural ferrous and sulfide moieties [28–30]. Importantly, the surface structure of Fe_3S_4 can be tuned by synthesis methods to enhance various functional applications [31–33]. In spite of the previous studies investigating iron-sulfide materials, there is a paucity of information regarding specific ·OH production pathways associated with Fe_3S_4 and the efficacy of utilizing ·OH production by Fe_3S_4 for oxidation of environmental pollutants.

Arsenic, as a redox metalloid, occurs naturally in soils and rocks and is widely used in industry and agriculture [34]. Due to the dissolution out of rock or industrial release, high levels of arsenic were often detected in ground water [35]. As the specific interaction of iron sulfides and As(III), and high stabilization of the formed As-Fe-S products [36], it is promising to involve Fe_3S_4 for As(III) removal. Herein, we aim to elucidate the effects of sulfur vacancies in Fe_3S_4 (greigite) on ·OH production mechanisms and As(III) removal under both oxic and anoxic conditions. Cumulative ·OH production from Fe_3S_4 was quantified via the probe reaction between benzoic acid (BA) and ·OH to generate *p*-hydroxybenzoic acid (*p*-HBA). A series of trapping agents were used to evaluate the contribution of reactive oxygen intermediates to ·OH production. Specific molecular probe experiments quantified the concentrations of iron species (Fe(II), Fe(III), and Fe(IV)) and reactive oxygen species to rigorously characterize reaction pathways. As such, this study provides fundamental mechanistic information concerning ·OH production pathways by Fe_3S_4 and highlights potential applications for environmental remediation.

2. Experimental section

2.1. Sample preparation

Sulfur-vacancy (SV) Fe_3S_4 nanosheets were synthesized using a one-step solvothermal method [31,37]. In the SV-rich Fe_3S_4 synthesis process, 0.834 g $FeSO_4{\cdot}7H_2O$ was dissolved in 30 mL of ethylene glycol (EG) to form solution *I*, and 0.363 g L-cysteine was dissolved in 30 mL of EG to form solution *II*. Solution *I* was added dropwise into solution *II* within 5 min and stirred at room temperature for 20 min to form a bright red mixture. The resulting solution was transferred into a 100 mL Teflon-lined stainless steel autoclave and heated at 180 °C for 12 h. After cooling to room temperature, a black product was collected by centrifugation and sequential washed with deionized water and ethanol three times before drying in a vacuum oven at 60 °C for 6 h. The SV-poor Fe_3S_4 was synthesized following identical methods, but using water rather than EG as the solvent.

2.2. ·OH production from Fe_3S_4

A mixed solution of benzoic acid/piperazine-N,N'-bis(2-ethane sulfonic acid) (BA/PIPES) was prepared by dissolving 1.220 g BA and 0.906 g PIPES into 1 L deionized water. PIPES were selected because they do not complex with Fe(III) and Fe(II). The pH of the mixture was adjusted to 6.7 ± 0.1 using 1 mM NaOH. This stock solution was stored in the dark to avoid potential photochemical reactions. Oxic experiments were carried out in 50 mL conical flasks containing 20 mL BA/PIPES stock solution and a desired dosage of Fe_3S_4. Flasks were covered with aluminum foil and shaken with a rotary shaker (SPH-100B, Shiping, China) at 150 rmp and 25 °C. For anoxic experiments, the BA/PIPES solution was purged with ultrapure argon gas for 1 h to remove dissolved oxygen, and then transferred into a two-necked flask. To avoid oxygen contamination in the reactor, the two-necked flask was connected with an argon filled balloon and rubber stopper.

Samples were withdrawn at a regular time interval from the flask with a 2-mL syringe. As the reaction rate constant for BA and ·OH ($k_{BA,·OH}$ = 5.7 × 10^9 $M^{-1}s^{-1}$) is much higher than that for PIPES and ·OH, the consumption of ·OH by PIPES was ignored [38]. Quenching experiments were carried out with additions of 2,2′-bipyridine (BPY, 10 mM), superoxide dismutase (SOD, 600 U/L) and catalase (CAT, 2450 U/L) to the reaction process. Samples were passed through a 0.22 μm polytetrafluoroethylene (PTFE) filter to remove residual Fe_3S_4. All experiments were carried out in triplicate.

2.3. As(III) oxidation by SV-rich Fe_3S_4

To demonstrate the application of ·OH production by SV-Fe_3S_4 for remediation of environmental pollutants, As(III) was selected as a model pollutant. Briefly, the As(III) standard solution was diluted into PIPES (3 mM, pH 6.7 ± 0.1) to form a 10 mg/L As(III) stock solution. A 0.02 g mass of SV-rich Fe_3S_4 and 40 mL As(III) stock solution were transferred into the aforementioned reactor under oxic or anoxic conditions. The reactor was shaken with a rotary shaker (SPH-100B, Shiping, China) at 150 rmp and 30 °C. Samples were passed through a 0.22 μm PTFE filter and 500 μL methanol (6 M) added to quench further reaction between As(III) and ·OH. All experiments were carried out in triplicate.

3. Results and discussion

3.1. Characterization of S-vacancy Fe_3S_4

Figure S1a shows powder X-ray diffraction (XRD) patterns for Fe_3S_4 synthesized using EG and H_2O as the solvent. Diffraction peaks for both samples are well indexed to the cubic phase of Fe_3S_4 (No.16-173), verifying successful synthesis of Fe_3S_4 crystals. As EG favors the formation of surface defects in nanomaterials [39], S vacancies were characterized using EPR spectra (Figure S1b). A typical signal with a *g* factor of 2.003 identifies the existence of S vacancies in Fe_3S_4 synthesized using EG and H_2O as solvent. Notably, the signal intensity of Fe_3S_4 synthesized using EG as solvent was much higher than that of Fe_3S_4 synthesized with H_2O solvent. These results document that SV-rich Fe_3S_4 and SV-poor Fe_3S_4 were obtained from the solvothermal synthesized process using EG and H_2O as solvents, respectively. The morphology of Fe_3S_4, characterized by scanning electron microscopy (SEM) and transmission electron microscope (TEM), exhibited a sheet-like character with a thickness of ~10 nm for both samples, and a distinct bending in the SV-rich Fe_3S_4 structure (Figure S2). These characterization results were consistent with our previous work [37].

3.2. ·OH production with SV-Fe_3S_4

The ·OH production by SV-Fe_3S_4 was quantified using BA/PIPES solution under oxic conditions. Cumulative ·OH production by SV-rich Fe_3S_4 gradually increased to 138.9 μM within 8 h (Fig. 1). In contrast, ·OH production for SV-poor Fe_3S_4 was below the detection limit (0.59 μM) of the high performance liquid chromatography (HPLC) method revealing the importance of sulfur vacancies in promoting ·OH production under oxic conditions. The Brunauer Emmett-Teller (BET) surface areas were calculated to be 20.0 and 17.7 m^2/g, for the SV-rich Fe_3S_4 and SV-poor Fe_3S_4, respectively, which were corresponded to the average pore volumes of 10.1 and 10.8 nm [37]. These slight differences of BET surface areas and average pore volumes between the SV-poor Fe_3S_4 and SV-rich Fe_3S_4 ruled out the specific contributions of surface area and pore volume to the ·OH formation efficiency. Moreover, cumulative ·OH production by SV-rich Fe_3S_4 under anoxic conditions gradually increased to 98.0 μM within 8 h, which was considerably lower than production (138.9 μM) under oxic conditions (Fig. 1). Cumulative ·OH production curves for SV-rich Fe_3S_4 under both oxic and anoxic conditions followed a pseudo-zero-order kinetic model. The apparent ·OH generation rate constant for SV-rich Fe_3S_4 under oxic conditions (19.3 ± 1.0 μM•h^{-1}) was 1.6 times greater than the rate under anoxic conditions (11.8 ± 0.4 μM•h^{-1}) (Table S1). Thus, we conclude that SV-rich Fe_3S_4 generates ·OH production under both oxic and anoxic conditions, but ·OH generation rates are a function of dissolved oxygen concentration.

The dependence of ·OH production on the dosage of SV-rich Fe_3S_4 was evaluated for Fe_3S_4 doses of 0.5–3.0 g/L. Cumulative ·OH concentrations increased with increasing reaction time to 8 h (Fig. 2). Final ·OH concentrations increased from 30.7 and 13.2 μM to 138.9 and 98.0 μM as SV-rich Fe_3S_4 dosage increased from 0.5 to 3.0 g/L under oxic and anoxic conditions, respectively (Table S2). These concentrations correspond to ·OH production rate increases from 3.9 ± 0.2 and 1.7 ± 0.2 μM•h^{-1} to 19.3 ± 1.0 and 11.8 ± 0.4 μM•h^{-1} (Table S2), respectively. The ·OH production rates under oxic and anoxic conditions were linearly dependent on the dosage of SV-rich Fe_3S_4 (Fig. 2c). The slope under oxic conditions (7.0 ± 0.8 μmol•h^{-1}•g^{-1}) was notably higher than for anoxic conditions (4.0 ± 0.1 μmol•h^{-1}•g^{-1}), indicating the importance of molecular oxygen in the reaction processes.

3.3. Mechanism of ·OH production by SV-rich Fe_3S_4

·OH can be generated with iron-based materials via three pathways: (1) a two-step single-electron transfer from Fe(II) to oxygen generating $·O_2^-$ and H_2O_2, with the H_2O_2 subsequently decomposed by Fe(II) via the Fenton reaction to generate ·OH; (2) a direct two-electron transfer from iron-based materials to oxygen generating H_2O_2 and subsequent Fenton reaction; and (3) the oxidation of H_2O to ·OH by surface defects or high-valence iron ions (such as Fe(IV)) [40]. To clarify the ·OH production mechanism(s) induced by SV-rich Fe_3S_4 under oxic and anoxic conditions, we applied different scavengers (SOD for $·O_2^-$, BPY for Fe(II), and CAT for H_2O_2) to capture the suspected reactive species involved in the ·OH production process. The ·OH production rates were not depressed in the presence of SOD under oxic conditions, suggesting that $·O_2^-$ was not an important component in the reaction pathway (Figure S3). Thus, we rule out the pathway for a direct two-step single-electron transfer from Fe(II) to oxygen for the generation of $·O_2^-$ and H_2O_2 by SV-rich Fe_3S_4 under oxic conditions. In contrast, ·OH

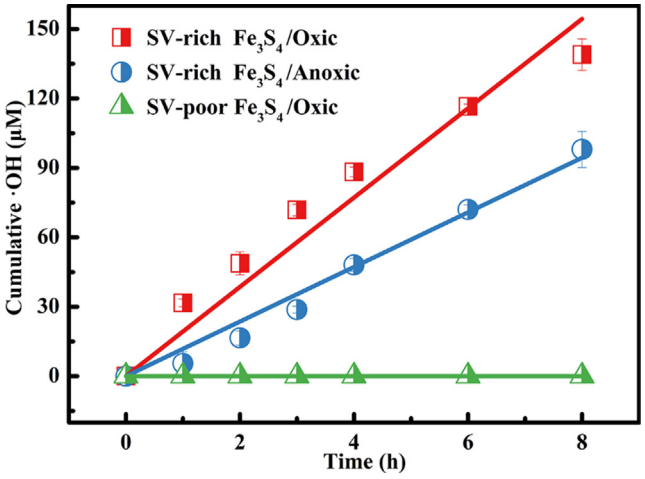

Fig. 1. Cumulative concentrations of ·OH under different conditions induced by S-vacancy Fe_3S_4. The dosage of Fe_3S_4 was 3.0 g/L.

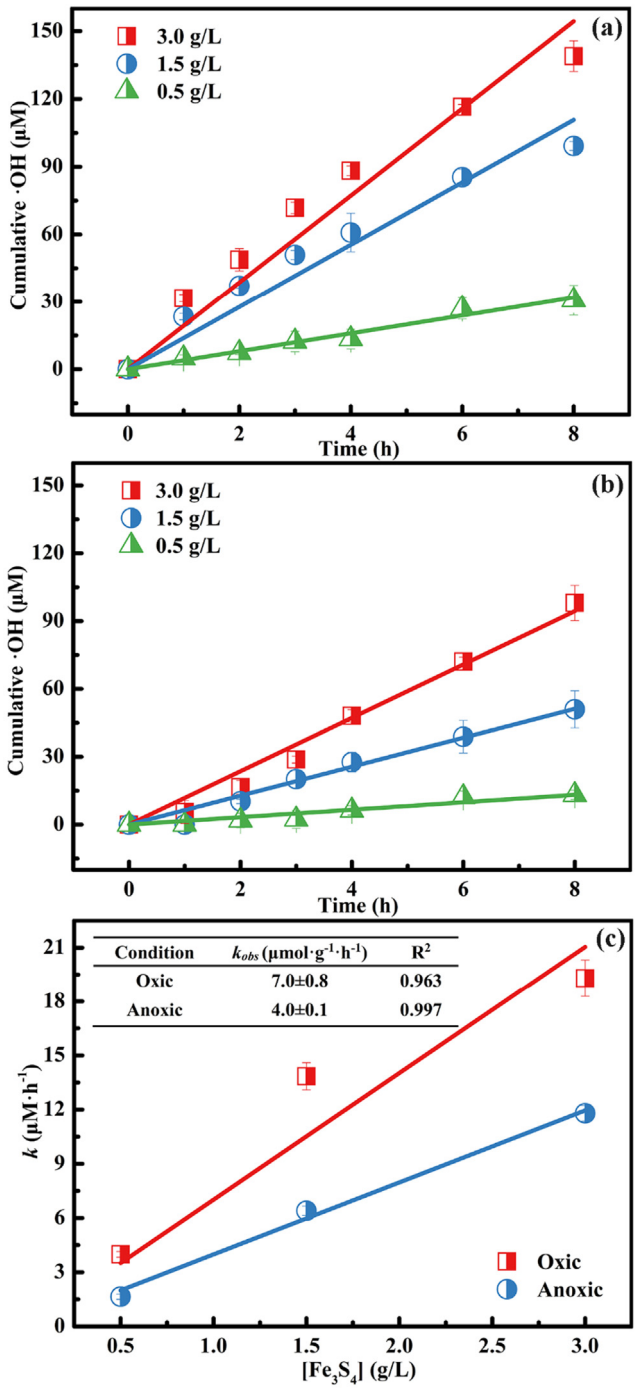

Fig. 2. Effects of SV-rich Fe_3S_4 dosage on the cumulative concentrations of ·OH under oxic (a) and anoxic (b) conditions; (c) Linear dependence of pseudo-zero-order rate constant for ·OH production as a function of SV-rich Fe_3S_4 dosage.

production rates markedly decreased from 19.3 ± 1.0 to 0.4 ± 0.2 and 1.6 ± 0.1 μM•h^{-1} with the addition of BPY and CAT, respectively (Fig. 3a and Table S3). This confirms that oxic ·OH production processes by SV-rich Fe_3S_4 involve Fe(II) and H_2O_2. These data provided compelling evidence that oxygen is efficiently activated by SV-rich Fe_3S_4 via a two-electron transfer route to generate H_2O_2 rather than a single-electron transfer route to generate $\cdot O_2^-$. Similarly, ·OH production rates under anoxic conditions were depressed by BPY and CAT (Fig. 3b), further revealing the significant role of Fe (II) and H_2O_2 in ·OH production in the absence of oxygen.

Next, we quantified the role of Fe species (Fe(II) and Fe(III)) in ·OH production pathways. Fe(II) concentrations increased from 0.003 and 0.004 to 0.696 and 0.490 mM at 8 h as the dosage of SV-rich Fe_3S_4 increased from 0.5 to 3.0 g/L under oxic and anoxic conditions, respectively (Figure S4). The higher Fe(II) concentration under oxic conditions was attributed to more efficient redox facilitated dissolution of SV-rich Fe_3S_4 in the presence of dissolved oxygen. Correspondingly, all Fe(III) concentrations under both oxic and anoxic conditions were lower than the detection limit (<0.007 mM) (Figure S5) owing to the low solubility of Fe(III) at pH 7.0.

To further evaluate the effects of iron species on ·OH production processes under oxic and anoxic conditions, the solid-phase products were separated and characterized by XPS. The high-resolution spectra of Fe 2p in pristine SV-rich Fe_3S_4 displayed four peaks at 707.6, 710.3, 711.5, and 712.8 eV (Figure S6), which were assigned to surface Fe(II)-S and structural Fe(II)-S, Fe(III)-S, and Fe(III)-O, respectively [41,42]. The relative fraction of $Fe(II)_{surf}$ decreased from 5.8% to 3.2% after anoxic reaction, indicating release and partial Fe(II) oxidization under anoxic conditions. Meanwhile, $Fe(II)_{surf}$ markedly disappeared after oxic reaction, suggesting enhanced oxidation of $Fe(II)_{surf}$ in the presence of oxygen. Correspondingly, the relative fraction of Fe(III)-O increased from 18.3% to 23.7% and 25.6% under anoxic and oxic conditions, respectively. The increase in Fe(III)-O confirms Fe(II) oxidation to generate Fe(III) in both oxic and anoxic pathways.

As H_2O_2 is a key intermediate for ·OH production via the Fenton reaction, we quantified H_2O_2 concentrations in BA/PIPES solution at SV-rich Fe_3S_4 dosages of 0.5–3.0 g/L under oxic and anoxic conditions·H_2O_2 concentrations sharply increased to 2.6, 1.6, and 2.0 μM at 2 h as the SV-rich Fe_3S_4 dosage increased from 0.5 to 3.0 g/L under oxic conditions (Fig. 3c). These results confirm the efficient production of H_2O_2 in the presence of SV-rich Fe_3S_4 and oxygen. Subsequently, H_2O_2 concentrations decreased to 0.9, 1.7 and 1.9 μM after 8 h of reaction as SV-rich Fe_3S_4 dosages increased. The prominent decrease in instantaneous H_2O_2 concentrations for the 0.5 g/L SV-rich Fe_3S_4 treatment indicates that the H_2O_2 generation rate induced by Fe_3S_4 was lower than the H_2O_2 decomposition rate via the Fenton reaction at lower Fe_3S_4 dosages. Instantaneous H_2O_2 concentrations were independent of SV-rich Fe_3S_4 mass at higher doses. This may result from rapid consumption of H_2O_2 via the Fenton reaction in the presence of high concentrations of Fe(II) released from redox promoted dissolution of SV-rich Fe_3S_4 at higher solid-phase concentrations. In contrast, instantaneous H_2O_2 concentrations gradually increased to ~0.7 μM for all SV-rich Fe_3S_4 dosages (0.5–3.0 g/L) under anoxic conditions (Fig. 3d). The H_2O_2 concentrations generated under anoxic conditions were notably lower than those under oxic conditions. Thus, we conclude that H_2O_2 generation induced by SV-rich Fe_3S_4 was strongly dependent on the dissolved oxygen concentration.

To further clarify the effects of H_2O_2 on ·OH production with SV-rich Fe_3S_4 under oxic and anoxic conditions, we evaluated ·OH production upon spiking with H_2O_2. The ·OH concentration increased from 138.9 to 241.3 μM with the addition of 5 mM H_2O_2 under oxic conditions (Fig. S7a). The large increase in ·OH concentration may be attributed to an enhancement of the Fenton reaction by increased availability of ferrous ions via redox promoted dissolution of SV-rich Fe_3S_4 in the presence of oxygen (Figure S4). In contrast, a much smaller increase in ·OH concentrations occurred (98.0 to 131.3 μM) upon addition of 5 mM H_2O_2 under anoxic conditions (Figure S7b). This differential response to H_2O_2 additions suggests a less important role for the Fenton reaction generation of ·OH under anoxic conditions.

Given the importance of dissolved oxygen (DO) in redox reactions, we monitored DO concentrations during ·OH production by SV-rich Fe_3S_4 under oxic and anoxic conditions using a DO probe (JPB-607A, Shanghai INESA). The initial DO concentration

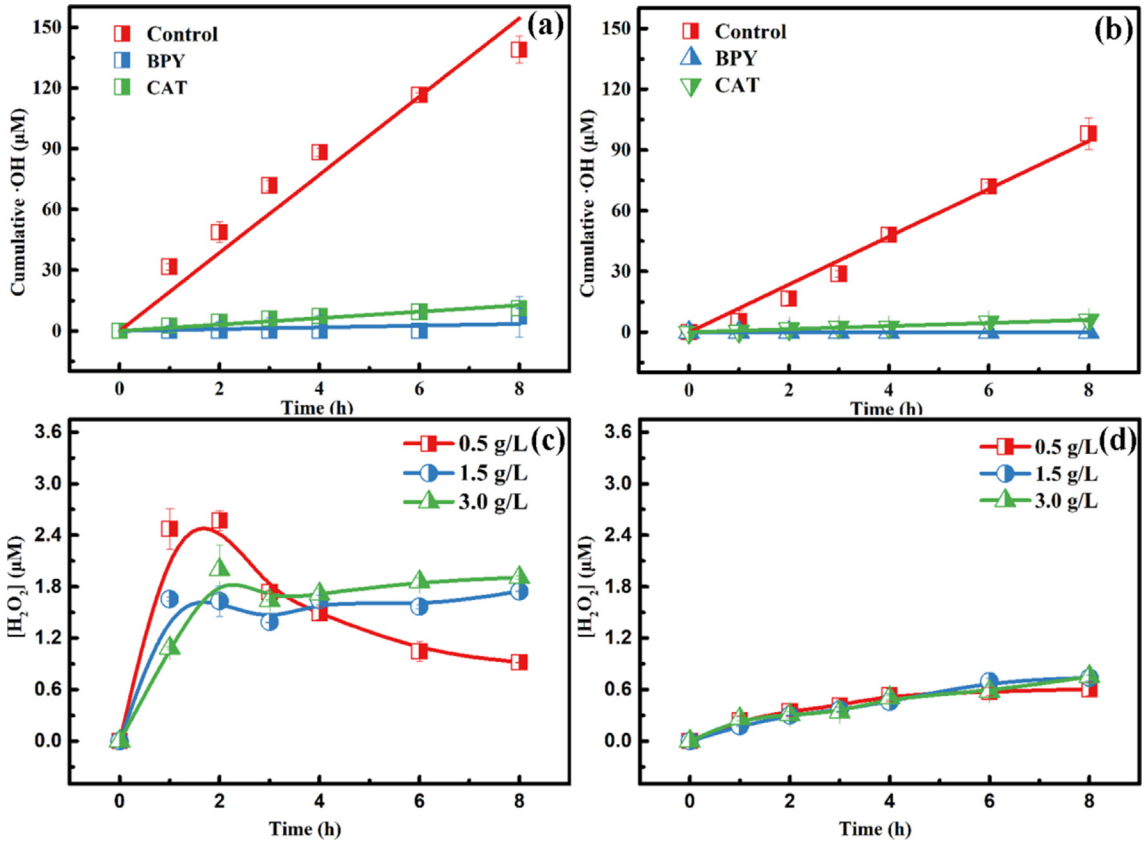

Fig. 3. Effects of inhibitors on cumulative ·OH concentrations induced by SV-rich Fe_3S_4 (3 g/L) under oxic (a) and anoxic (b) conditions; concentrations of SOD, BPY and CAT were 600 U/L, 10 mM and 2450 U/L, respectively. Time profiles of H_2O_2 concentration at different SV-rich Fe_3S_4 dosages under oxic (c) and anoxic (d) conditions.

(8.3 mg/L) was up to its saturated concentration (8.3 mg/L) at 25 °C, confirming the undersaturated of DO in the solution. However, it decreased to 7.4 mg/L after 1 h and maintained a concentration of 7.2 ± 0.2 mg/L for the remaining 7 h of reaction in the system open to the atmosphere (Figure S8). The initial decrease in DO was caused by the higher oxygen-consumptive rate than the reaeration rate into the reaction chamber. To further demonstrate oxygen consumption by reactions with SV-rich Fe_3S_4, we constrained the open system with a rubber stopper to record oxygen consumption. In the isolated system, DO concentration gradually decreased to ~ 5.0 mg/L within 8 h. These results confirmed the role of molecular oxygen in ·OH production by SV-rich Fe_3S_4 under oxic conditions.

DO concentrations were also monitored under anoxic conditions to follow ·OH production by SV-rich Fe_3S_4. DO concentrations were lower than 0.5 mg/L throughout the 8 h reaction period providing confirmation that molecular oxygen is not required for ·OH production in the SV-rich Fe_3S_4 system (Figure S8). The production of ·OH in the SV-rich Fe_3S_4 system under anoxic conditions probably acquires an oxygen atom from H_2O molecules. To verify this assumption, we examined the isotopic distribution of *p*-HBA obtained from the reaction of $H_2^{18}O$-enriched solution and SV-rich Fe_3S_4 in the BA/PIPES system under anoxic conditions. The prominent ion peak at *m*/*z* of 141.0543 confirmed that *p*-HBA-^{18}O was generated when using $H_2^{18}O$ as the solvent (Figure S9). These results confirm that the oxidation of H_2O was the source of the oxygen used to generate ·OH in the SV-rich Fe_3S_4 system under anoxic conditions.

Finally, we examined whether H_2O was oxidized to generate ·OH by ferryl ions (Fe(IV)) in association with the sulfur defects on iron-based materials. Methyl phenyl sulfoxide (PMSO) was used as a molecular probe for detection of Fe(IV) during the SV-Fe_3S_4 oxidation process [43]. HPLC chromatograms revealed a new peak with a retention time of 6.8 min that matched the $PMSO_2$ standard solution (Figure S10). These results provide strong support for the generation of Fe(IV) released from SV-rich Fe_3S_4. $PMSO_2$ concentrations gradually increased to 7.2 and 4.9 μM within 8 h in the presence of SV-rich Fe_3S_4 under both oxic and anoxic conditions (Fig. 4). The higher Fe(IV) concentrations are consistent with the higher ·OH concentrations generated in the presence of oxygen. In sharp contrast, $PMSO_2$ concentrations were lower than 2.3 μM when using SV-poor Fe_3S_4 under oxic and anoxic conditions. This indicates that Fe(IV) is preferentially generated by SV-rich Fe_3S_4 providing strong evidence that both surface defects and oxygen favor Fe(IV) release from Fe_3S_4.

Synthesizing our results, we propose mechanistic pathways for production of ·OH by SV-rich Fe_3S_4 under oxic and anoxic conditions (Scheme 1). First, Fe(IV) released from SV-rich Fe_3S_4 directly oxidizes H_2O to generate ·OH under both oxic and anoxic conditions. Subsequently, the ·OH partially self-binds to form H_2O_2. Under oxic conditions, SV-rich Fe_3S_4 further donates electrons to oxygen molecules to generate H_2O_2. The H_2O_2 generated by these processes is finally decomposed by Fe(II) to produce ·OH via the Fenton reaction.

3.4. Removal of As(III) by reaction with SV-rich Fe_3S_4

To demonstrate the potential for oxidation of environmental pollutants by ·OH, we systematically investigated As(III) removal by SV-rich Fe_3S_4 under oxic and anoxic conditions. As(III) concentrations sharply decreased from 10 to ~ 0.01 mg/L within 120 min under both oxic and anoxic conditions (Fig. 5a). As As

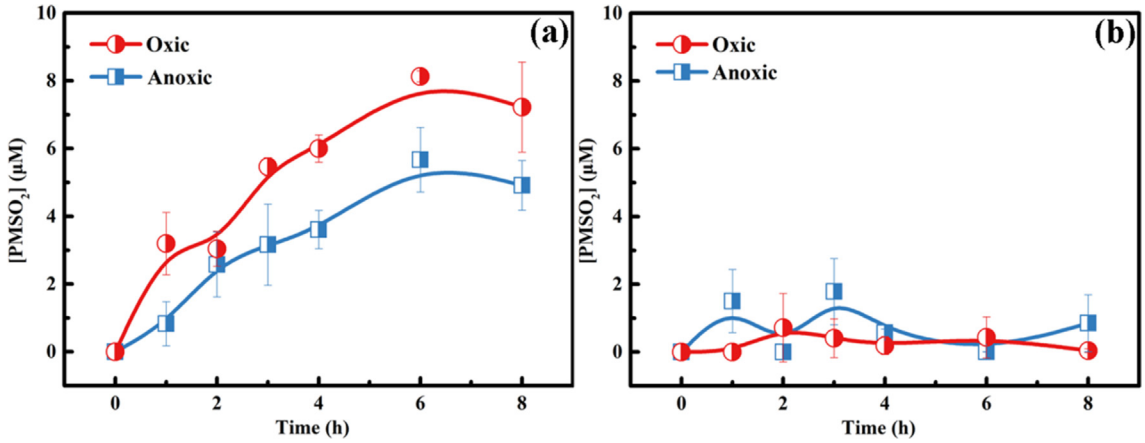

Fig. 4. Time profiles of $PMSO_2$ concentration with SV-Fe_3S_4 (3 g/L) under oxic and anoxic conditions: (a) SV-rich Fe_3S_4; (b) SV-poor Fe_3S_4. The initial concentration of PMSO was 10.0 mM.

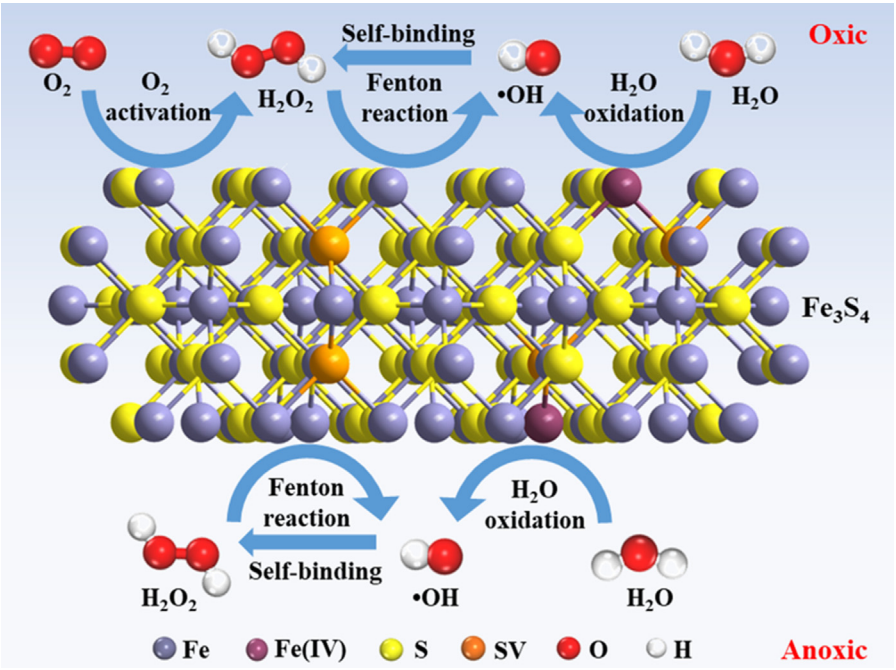

Scheme 1. Proposed ·OH generation mechanism with SV-Fe_3S_4 under oxic and anoxic conditions.

(III) removal by heterogeneous materials involves adsorption, oxidation and co-precipitation processes, dissolved As(V) concentrations were monitored throughout the reaction period. In all cases, dissolved As(V) concentrations were less than the detection limit (0.01 μg/L), indicating negligible accumulation of As(V) in the solution phase, but rather As retention on the solid-phase. After that, the contributions of different reactive species to As(III) removal were subsequently investigated in detail. Figure S11 shows that As(III) could not be removed with H_2O_2 alone under oxic and anoxic conditions, ruling out the direct oxidation of As (III) with H_2O_2. Furthermore, under oxic conditions, the As(III) removal efficiencies with SV-rich Fe_3S_4 were 59.3% and 61.3%, respectively, in the presence of methanol and isopropanol. Correspondingly, they were 59.2% and 60.2%, respectively, under anoxic conditions. Consequently, we posit that partial As(III) could be efficiently adsorbed or oxidized on the surface of SV-rich Fe_3S_4 surface, and As(III) oxidation mainly resulted from ·OH rather than Fe(IV).

To assess As interactions with the SV-rich Fe_3S_4 surface, the solid-phase was isolated following reaction and then reacted with a phosphate solution to desorb surface bound As(III) and As(V). The masses of As(III) and As(V) desorbed from the SV-rich Fe_3S_4 surface under oxic conditions were 12.5 and 25.5 μg, respectively (Fig. 5b). The higher concentration of As(V) than As(III) confirms the significant contribution of As(III) oxidation in the overall As(III) removal process. Under anoxic conditions, the masses of As(III) and As(V) desorbed from the SV-rich Fe_3S_4 were 18.1 and 3.3 μg, respectively. Thus, under anoxic conditions, As(III) is preferentially adsorb on the SV-rich Fe_3S_4 surface rather than being oxidized to As(V) and subsequently adsorbed. The lower mass of As(V) desorbed under anoxic conditions confirms the lower oxidative ability of SV-rich Fe_3S_4 under anoxic conditions. These findings are fully consistent with ·OH production dynamics with SV-rich Fe_3S_4 under oxic and anoxic conditions.

Importantly, the mass of total As desorbed from SV-rich Fe_3S_4 surfaces under anoxic (21.3 μg) and oxic (38.0 μg) conditions

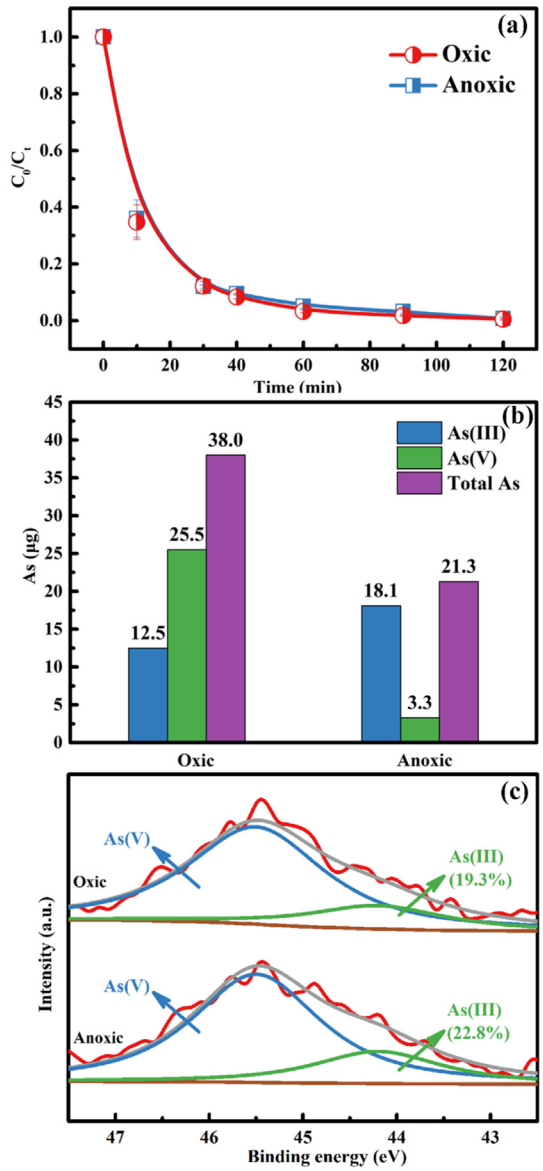

Fig. 5. (a) Time profiles of As(III) concentration upon reaction with SV-rich Fe_3S_4 under oxic and anoxic conditions; (b) Concentrations of As(III), As(V) and total As desorbed by phosphate from reacted SV-rich Fe_3S_4 under oxic and anoxic conditions; (c) As 3d XPS spectra of reacted SV-rich Fe_3S_4 under oxic and anoxic conditions. Initial concentrations of As(III) and SV-rich Fe_3S_4 were 10.0 mg/L and 0.5 g/L, respectively.

was much lower than the fortified As mass (200 μg). This discrepancy suggests the formation of other As-containing species (*i.e.*, strongly surface bound or co-precipitated phases) on the surface of the SV-rich Fe_3S_4. To distinguish surface associated As materials, the reacted SV-rich Fe_3S_4 was collected and characterized by XPS. The XPS spectra of As 3d was fitted by individual curves with peaks at 45.5 and 44.2 eV, attributable to As(V) and As(III), respectively (Fig. 5c) [44]. This analysis corroborates a higher relative fraction of As(V) under oxic (80.7%) than anoxic (77.2%) conditions and reflects the strong As(III) oxidative ability of SV-rich Fe_3S_4, especially under oxic conditions. Therefore, SV-rich Fe_3S_4 has the remarkable capacity to oxidize and retain As under both oxic and anoxic conditions.

4. Conclusions

In summary, this study demonstrated that magnetic Fe_3S_4 with sulfur vacancies achieved high ·OH production rates and As(III) oxidation/retention capabilities under both anoxic and oxic conditions. To further the application of SV-Fe_3S_4 for environmental applications, we systematically elucidated the ·OH production mechanisms and its efficacy for As(III) remediation. Experimental results confirmed that sulfur vacancies accelerated the formation of high-valent iron that in turn facilitated the direct oxidation of H_2O to produce ·OH under anoxic conditions. Additionally, structural ferrous ions in Fe_3S_4 activate molecular O_2 to generate H_2O_2 and promote subsequent Fenton reaction for ·OH production. This work enhances our mechanistic understanding of ·OH production and As(III) oxidation/retention and highlights the prospects of synthesizing structurally-defective, iron-based minerals to optimize remediation strategies. These ·OH-generating minerals have excellent potential for several environmental remediation applications, such as treatment of As(III)-polluted wastewater and degradation/-transformation of organic pollutants.

CRediT authorship contribution statement

Wei Liu: Conceptualization, Methodology, Investigation, Writing – original draft, Funding acquisition. **Jia Liu:** Investigation, Validation, Visualization. **Peipei Zhou:** Software, Formal analysis. **Randy A. Dahlgren:** Writing – review & editing. **Xuedong Wang:** Funding acquisition, Project administration, Supervision, Writing – review & editing.

Declaration of Competing Interest

The authors declare that they have no known competing financial interests or personal relationships that could have appeared to influence the work reported in this paper.

Acknowledgements

This work was jointly supported by National Science Foundation of China (Grants 21707105 and 22076134), Zhejiang Province Public Welfare Technology Application Research (Grant LGF19B070009), Natural Science Foundation of Jiangsu Province (Grant SBK2021022437), Key Science and Technology Project of Suzhou City (Grant SS202028), and Science Research Foundation of Wuhan Institute of Technology (Grant K2021007).

Appendix A. Supplementary material

Supplementary data to this article can be found online at https://doi.org/10.1016/j.jcis.2021.08.072.

References

[1] D. Rickard, B. Hatton, D.M. Murphy, I.B. Butler, A. Oldroyd, A. Hann, FeS-induced radical formation and its effect on plasmid DNA, Aquat. Geochem. 17 (2011) 545–566.
[2] M. Tong, S. Yuan, S. Ma, M. Jin, D. Liu, D. Cheng, X. Liu, Y. Gan, Y. Wang, Production of abundant hydroxyl radicals from oxygenation of subsurface sediments, Environ. Sci. Technol. 50 (2016) 214–221.
[3] S.C. Ma, M. Tong, S.H. Yuan, H. Liu, Responses of the microbial community structure in Fe(II)-bearing sediments to oxygenation: The role of reactive oxygen species, ACS Earth Space Chem. 3 (2019) 738–747.
[4] A.D. Harrington, S. Hylton, M.A.A. Schoonen, Pyrite-driven reactive oxygen species formation in simulated lung fluid: Implications for coal workers' pneumoconiosis, Environ. Geochem. Hlth. 34 (2012) 527–538.

[5] M.A.A. Schoonen, A.D. Harrington, R. Laffers, D.R. Strongin, Role of hydrogen peroxide and hydroxyl radical in pyrite oxidation by molecular oxygen, Geochim. Cosmochim. Acta 74 (2010) 4971–4987.
[6] R.T. Lowson, Aqueous oxidation of pyrite by molecular oxygen, Chem. Rev. 82 (1982) 461–497.
[7] Y. Mu, F.L. Jia, Z.H. Ai, L.Z. Zhang, Molecular oxygen activation with nano zero-valent iron for aerobic degradation of organic contaminants and the performance enhancement, Acta Chim. Sinica 75 (2017) 538–543.
[8] W. Liu, L. Jin, K. Chen, Y. Li, R.A. Dahlgren, M. Ma, X. Wang, Inhibitory effects of natural organic matter on methyltriclosan photolysis kinetics, RSC Adv. 8 (2018) 21265–21271.
[9] M.A.A. Schoonen, C.A. Cohn, E. Roemer, R. Laffers, S.R. Simon, T. O'Riordan, Mineral-induced formation of reactive oxygen species, Rev. Mineral. Geochem. 64 (2006) 179–221.
[10] S.H. Joo, A.J. Feitz, T.D. Waite, Oxidative degradation of the carbothioate herbicide, molinate, using nanoscale zero-valent iron, Environ. Sci. Technol. 38 (2004) 2242–2247.
[11] C.A. Cohn, S.C. Fisher, B.J. Brownawell, M.A.A. Schoonen, Adenine oxidation by pyrite-generated hydroxyl radicals, Geochem. Trans. 11 (2010) 2.
[12] L. Wang, M. Cao, Z. Ai, L. Zhang, Dramatically enhanced aerobic atrazine degradation with Fe@Fe_2O_3 core-shell nanowires by tetrapolyphosphate, Environ. Sci. Technol. 48 (2014) 3354–3362.
[13] S.H. Yuan, X.X. Liu, W.J. Liao, P. Zhang, X.M. Wang, M. Tong, Mechanisms of electron transfer from structrual Fe(II) in reduced nontronite to oxygen for production of hydroxyl radicals, Geochim. Cosmochim. Acta 223 (2018) 422–436.
[14] W. Liu, Y.Y. Wang, Z.H. Ai, L.Z. Zhang, Hydrothermal synthesis of FeS_2 as a high-efficiency Fenton reagent to degrade alachlor via superoxide-mediated Fe(II)/Fe(III) cycle, ACS Appl. Mater. Interfaces 7 (2015) 28534–28544.
[15] W. Liu, Z. Ai, M. Cao, L. Zhang, Ferrous ions promoted aerobic simazine degradation with Fe@Fe_2O_3 core–shell nanowires, Appl. Catal. B: Environ. 150–151 (2014) 1–11.
[16] P. Zhang, S.H. Yuan, Production of hydroxyl radicals from abiotic oxidation of pyrite by oxygen under circumneutral conditions in the presence of low-molecular-weight organic acids, Geochim. Cosmochim. Acta 218 (2017) 153–166.
[17] M.J. Borda, A.R. Elsetinow, D.R. Strongin, M.A. Schoonen, A mechanism for the production of hydroxyl radical at surface defect sites on pyrite, Geochim. Cosmochim. Acta 67 (2003) 935–939.
[18] L. Kong, X. Hu, M. He, Mechanisms of Sb(III) oxidation by pyrite-induced hydroxyl radicals and hydrogen peroxide, Environ. Sci. Technol. 49 (2015) 3499–3505.
[19] S. Diem, O.A. Cirpka, M. Schirmer, Modeling the dynamics of oxygen consumption upon riverbank filtration by a stochastic–convective approach, J. Hydrol. 505 (2013) 352–363.
[20] P. Zhang, S. Yuan, P. Liao, Mechanisms of hydroxyl radical production from abiotic oxidation of pyrite under acidic conditions, Geochim. Cosmochim. Acta 172 (2016) 444–457.
[21] I. Snowball, R. Thompson, The occurrence of greigite in sediments from Loch Lomond, J. Quaternary Sci. 3 (1988) 121–125.
[22] F. Demory, H. Oberhansli, N.R. Nowaczyk, M. Gottschalk, R. Wirth, R. Naumann, Detrital input and early diagenesis in sediments from Lake Baikal revealed by rock magnetism, Global Planet. Change 46 (2005) 145–166.
[23] S. Hunger, L.G. Benning, Greigite: A true intermediate on the polysulfide pathway to pyrite, Geochem. Trans 8 (2007) 1–20.
[24] Y. Ai, G. Liu, H. Wang, C. Wu, W. Liu, Z. Lin, Role of sulfur atoms in the adsorption of antimony by greigite, Surf. Interfaces 20 (2020) 100584.
[25] L. Kong, Z. Li, X. Huang, S. Huang, H. Sun, M. Liu, L. Li, Efficient removal of Pb(II) from water using magnetic Fe_3S_4/reduced graphene oxide composites, J. Mater. Chem. A 5 (2017) 19333–19342.
[26] Y.B. Shi, X.B. Wang, X.F. Liu, C.C. Ling, W.J. Shen, L.Z. Zhang, Visible light promoted Fe_3S_4 Fenton oxidation of atrazine, Appl. Catal. B: Environ. 277 (2020) 119229.
[27] X. Lin, K. Shih, J. Chen, X. Xie, Y. Zhang, Y. Chen, Z. Chen, Y. Li, Insight into flower-like greigite-based peroxydisulfate activation for effective bisphenol A abatement: Performance and electron transfer mechanism, Chem. Eng. J. 391 (2019) 123558.
[28] W. Liu, Z.H. Ai, R.A. Dahlgren, L.Z. Zhang, X.D. Wang, Adsorption and reduction of roxarsone on magnetic greigite (Fe_3S_4): Indispensable role of structural sulfide, Chem. Eng. J. 330 (2017) 1232–1239.
[29] W. Liu, L. Jin, J. Xu, J. Liu, Y. Li, P. Zhou, C. Wang, R.A. Dahlgren, X. Wang, Insight into pH dependent Cr(VI) removal with magnetic Fe_3S_4, Chem. Eng. J. 359 (2019) 564–571.
[30] X. Wang, J. Xu, J. Liu, J. Liu, F. Xia, C. Wang, R.A. Dahlgren, W. Liu, Mechanism of Cr(VI) removal by magnetic greigite/biochar composites, Sci. Total Environ. 700 (2020) 134414.
[31] S. Shit, W. Jang, S. Bolar, N.C. Murmu, H. Koo, T. Kuila, Effect of the solvent ratio (ethylene glycol/water) on the preparation of an iron sulfide electrocatalyst and its activity towards overall water splitting, Chem. Electro. Chem. 6 (2019) 3199–3208.
[32] Z. Duan, Q. Liu, C. Gai, X. Zhao, Magnetostratigraphic and environmental implications of greigite (Fe_3S_4) formation from Hole U1433A of the IODP Expedition 349, South China Sea. Mar. Geol. 394 (2017) 82–97.
[33] M. Wu, X. Zhou, S. Huang, J. Cheng, Z. Ding, A first-principles study of the effect of vacancy defects on the electronic structures of greigite (Fe_3S_4), Sci. Rep. 8 (2018) 11408.
[34] T. Shi, H. Liu, Y. Chen, J. Wang, G. Wu, Estimation of arsenic in agricultural soils using hyperspectral vegetation indices of rice, J. Hazard. Mater. 308 (2016) 243–252.
[35] B. Dousova, F. Buzek, M. Lhotka, S. Krejcova, R. Boubinova, Leaching effect on arsenic mobility in agricultural soils, J. Hazard. Mater. 307 (2016) 231–239.
[36] J. Cantu, L.E. Gonzalez, J. Goodship, M. Contreras, M. Joseph, C. Garza, T.M. Eubanks, J.G. Parsons, Removal of arsenic from water using synthetic Fe7S8 nanoparticles, Chem. Eng. J. 290 (2016) 428–437.
[37] W. Liu, J. Tian, C. Mao, Z. Wang, J. Liu, R.A. Dahlgren, L. Zhang, X. Wang, Sulfur vacancy promoted peroxidase-like activity of magnetic greigite (Fe_3S_4) for colorimetric detection of serum glucose, Anal. Chim. Acta 1127 (2020) 246–255.
[38] G.V. Buxton, C.L. Greenstock, W.P. Helman, A.B. Ross, Critical review of rate constants for reactions of hydrated electrons, hydrogen atoms and hydroxyl radicals (•OH/•O^-) in aqueous solution, J. Phys. Chem. Ref. Data 17 (1988) 513–886.
[39] J. Liao, L. Chen, M. Sun, B. Lei, X. Zeng, Y. Sun, F. Dong, Improving visible-light-driven photocatalytic NO oxidation over BiOBr nanoplates through tunable oxygen vacancies, Chinese J. Catal. 39 (2018) 779–789.
[40] S.Y. Pang, J. Jiang, J. Ma, Technology, Oxidation of sulfoxides and arsenic(III) in corrosion of nanoscale zero valent iron by oxygen: evidence against ferryl ions (Fe(IV)) as active intermediates in Fenton reaction, Environ. Sci. Technol. 45 (2011) 307–312.
[41] A.G. Schaufu, H.W. Nesbitt, I. Kartio, K. Laajalehto, G.M. Bancroft, R. Szargan, Incipient oxidation of fractured pyrite surfaces in air, J. Electron Spectros. 96 (1998) 69–82.
[42] C.F. Jones, S. Lecount, R.S.C. Smart, T.J. White, Compositional and structural alteration of pyrrhotite surfaces in solution: XPS and XRD studies, Appl. Surf. Sci. 55 (1992) 65–85.
[43] Z. Wang, J. Jiang, S. Pang, Y. Zhou, C. Guan, Y. Gao, J. Li, Y. Yang, W. Qiu, C. Jiang, Is sulfate radical really generated from peroxydisulfate activated by iron(II) for environmental decontamination?, Environ Sci. Technol. 52 (2018) 11276–11284.
[44] X. Han, J. Song, Y.L. Li, S.Y. Jia, W.H. Wang, F.G. Huang, S.H. Wu, As(III) removal and speciation of Fe (Oxyhydr)oxides during simultaneous oxidation of As(III) and Fe(II), Chemosphere 147 (2016) 337–344.